Comment on "Single Crystals of Single-Walled Carbon Nanotubes Formed by Self-Assembly"

Schlittler *et al.* (*1*) reported the production of single crystals of single-walled carbon nanotubes (SWCNTs) by the thermolysis of nanopatterned structures of alternating layers of C_{60} and nickel. Electron diffraction, high-resolution phase contrast imaging, and electron energy loss spectroscopy (EELS) were used to characterize the resulting crystals. In this comment, we report the reproduction of their experimental results; however, we disagree with their interpretation of the data. We suggest that the crystals formed in our experiments consist not of SWCNTs, but rather of calcium molybdenum oxide.

Multilayered structures, around 100 nm tall (300 nm in diameter) and consisting of 11 alternating layers of Ni and C_{60}, were patterned on Mo transmission electron microscopy (TEM) grids (Fig. 1A) in a special vacuum evaporation apparatus (*2*) as described in (*1*). The patterned grids were annealed inside a TEM microscope (Philips 400) using a heating holder (Gatan 652). The estimated magnetic field in this arrangement was on the order of 1 T; however, other annealing treatments ranged from no applied field up to a field of 7 T (*3*). The grids were typically outgassed at 200°C for 10 min and then ramped at 20°C/min to temperatures of 900 to 1000 °C.

The results of numerous annealing experiments can be summarized as follows: No faceted crystals were observed emerging from the multilayer stacks, which assumed a variety of interesting morphologies (Fig. 1B). However, long, thin nanocrystals matching the description in (*1*) were randomly scattered on the grids—that is, found in regions of the grids that were free of any deposited structures (Fig. 1C). These were easily distinguishable from the short, stubby, nanocrystals that were observed on etched regions on unannealed, as-received Mo TEM grids (as shown in Fig. 1A). Finding the long nanocrystals so far from the patterned multilayer stacks suggested that the two were unrelated, so as-received Mo TEM grids (300 mesh, EMS) were subjected to the same annealing treatment (950°C), and long, thin, nanocrystals were again obtained. No effect of magnetic field on either the occurrence or the orientation of the nanocrystals was observed.

These long, platelike crystals typically had a high aspect ratio and faceted ends. When examined in situ or ex situ using a 100-kV conventional TEM, the longitudinal fringes reported in (*1*) were usually observed (Fig. 2, A and B). Longitudinal fringes with spacings around 1-nm were also observed (Fig. 2, C and D) in Z-contrast images from a 100 kV scanning transmission electron microscope (STEM) equipped with a high-angle, annular dark-field (HAADF) detector (VG Instruments HB501UX). Z-contrast images taken at higher magnification revealed a complex atomic structure with alternating light and dark fringes (Fig. 2D) and—an important observation—lattice fringes parallel to the facets of the crystals.

Simultaneous electron energy loss (EEL) spectra were acquired during Z-contrast imaging. In a typical EEL spectrum from near the edge of a nanocrystal (Fig. 2E), the so-called

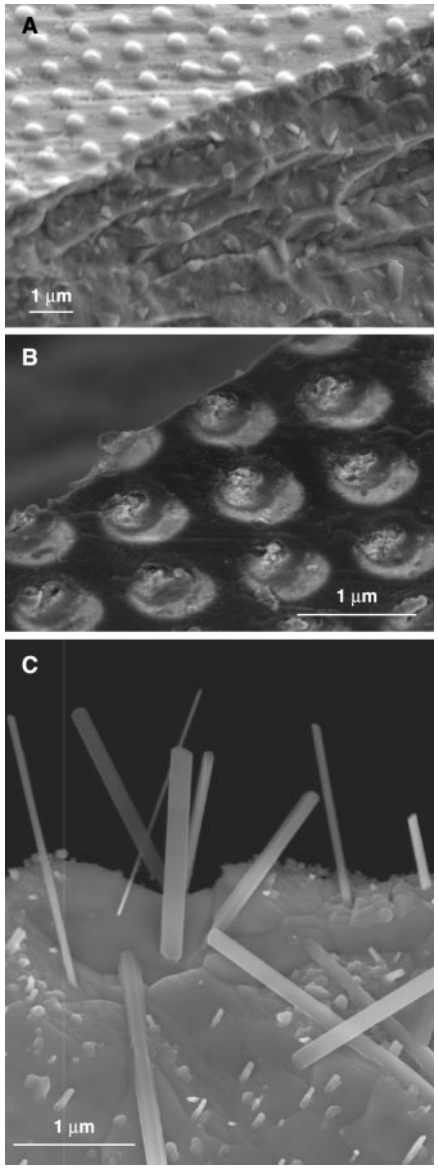

Fig. 1. C_{60}/Ni multilayer stacks patterned on a Mo TEM grid (**A**) before and (**B**) after thermolysis. (**C**) Faceted crystals observed on regions of Mo TEM grids (away from the multilayer stacks) after thermolysis treatments.

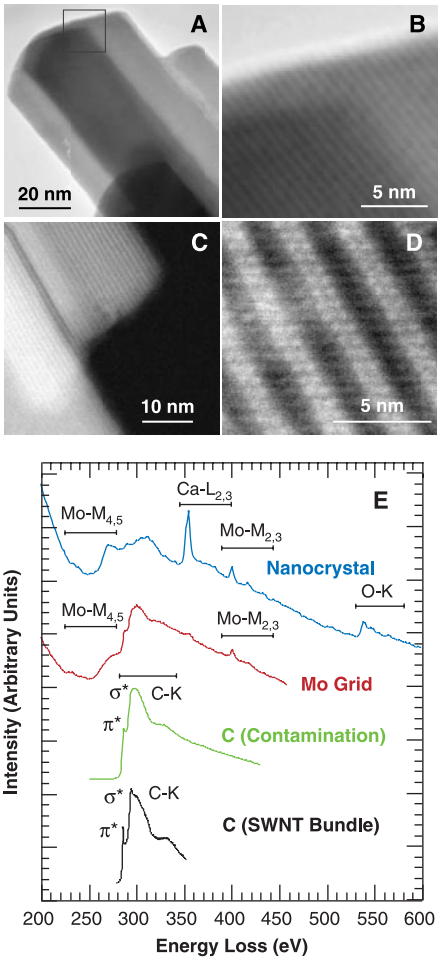

Fig. 2. (**A**) Bright-field TEM image of long, faceted crystals observed after annealing. (**B**) Enlarged view of region indicated by red square in (**A**), showing longitudinal fringes observed parallel to the long axis of the crystals. (**C** and **D**) HAADF (Z-contrast) STEM images show longitudinal fringes and reveal crystal planes parallel to facets. (**E**) Typical EEL spectra from a typical nanocrystal shows Mo, Ca, O, and possible C. An EEL spectrum from the Mo grid near the nanocrystal is shown for comparison. C from contamination on the edge of the nanocrystal is similar to the spectrum in (*1*), but is not representative of graphitized C as expected from SWCNT (a spectrum from SWCNT bundles produced by laser vaporization is shown for comparison).

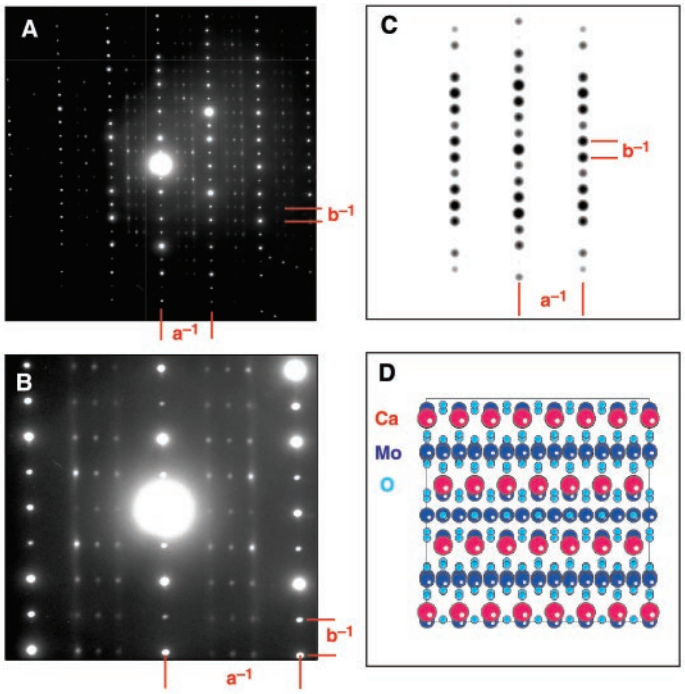

Fig. 3. (**A**) Electron diffraction pattern from crystal with longitudinal fringes. (**B**) Enlarged view yielding major lattice spacings a = 2.6 Å, b = 10.1 Å, and superlattice reflections at 1/3, 1/2, and 2/3 of reciprocal lattice spacing a^{-1}. (**C**) Simulated electron diffraction pattern from the projection of the $Ca_{5.45}Mo_{18}O_{32}$ structure shown in (**D**), in which a = 2.8 Å, b = 11.4 Å.

π* peak, characteristic of sp^2-bonded carbon, is clearly visible, as in (*1*). However, despite the suggestion to the contrary in (*1*), this feature cannot be used to infer the presence of graphite-like sheets in the sample. For comparison, an EEL spectrum recorded under similar conditions from a bundle of SWCNTs (grown by laser vaporization) is also shown in Fig. 2E. Although the π* peak is still present, the shape of the larger peak (known as the σ* peak) differs significantly between the two spectra, with more features visible in the latter owing to their graphene-based structure. A comparison of the C-K edges in Fig. 2E [and figure 2 in (*1*)] with spectra from different forms of carbon (*4*, *5*) suggests that the carbon signal from the crystals is due to amorphous carbon rather than to carbon nanotubes. Because the carbon signal was strongest at the edges of the nanocrystals, the amorphous carbon is believed to be predominantly surface contamination and not a major constituent of the crystals. An EEL spectrum from a typical nanocrystal (Fig. 2E) shows that the main elements in the nanocrystals are Ca, Mo and O (*6*).

Nanocrystals with longitudinal fringes produced electron diffraction (ED) patterns (Fig. 3, A and B) that were very similar to that published in (*1*). The basic unit of the pattern consisted of intense spots in roughly-perpendicular directions, with additional, weaker superlattice reflections located at 1/3, 1/2, and 2/3 of the larger reciprocal lattice spacing (a^{-1} in Fig. 3). Tilting the crystals over orthogonal axes varied the observed ED lattice spacings from $0.15 < a < 0.3$ nm and $0.5 < b < 1.02$ nm. These diffraction results indicate that the crystals are composed of widely separated layers of complicated atomic arrangements.

The structures of several molybdenum oxides intercalated with calcium are consistent with these diffraction results and the EELS results discussed earlier. The stable phase of MoO_3 has a layered structure in which MoO_6 octahedra connect at shared corners and edges in one plane, leaving a layered structure in the perpendicular direction. This structure is easily modified by the insertion of a wide variety of cations in the empty interstices of the interlayer region (*7*). A number of calcium molybdenum oxide phases are known to exist (*8*). From the ternary phase diagram, the most likely compound to form in a Mo-rich and Ca-poor environment with the observed d-spacings is $Ca_{5.45}Mo_{18}O_{32}$ (Fig. 3D). Using atomic coordinates for this compound (*9, 10*), simulations of dynamical diffraction patterns (Fig. 3C) reproduce most of the electron diffraction features observed experimentally (*11*). The only major features not reproduced in the simulations are the superlattice reflections at the 1/3, 1/2, and 2/3 positions, which the study of Schlittler *et al.* (*1*) also did not reproduce (*12*).

In view of these data, we suggest that the single crystals reported by Schlittler *et al.* (*1*) were not composed of SWCNTs, but rather represented molybdenum oxide intercalated with calcium. These crystals formed as the result of heating the molybdenum substrate in an oxygen-containing environment. Calcium, a common surface contaminant, is readily incorporated between molybdenum oxide layers. Under the appropriate conditions, thermolysis of condensed-phase precursors has been shown to grow carbon nanotubes (*13*, *14*). As the experiments in (*1*) and the reproduction of those experiments reported here shows, however, the introduction of reactive substrates and contaminants can result in nanocrystals with most unexpected compositions.

Matthew F. Chisholm
Oak Ridge National Laboratory
Post Office Box 2008
Oak Ridge, TN 37831, USA

Yuhuang Wang
Center for Nanoscale Science and Technology
Rice University
Houston, TX 77005, USA

Andrew R. Lupini
Gyula Eres
Alex A. Puretzky
Oak Ridge National Laboratory

Bruce Brinson
Center for Nanoscale Science and Technology
Rice University

Anatoli V. Melechko
David B. Geohegan*
Hongtao Cui
Oak Ridge National Laboratory

Marie P. Johnson
Center for Nanoscale Science and Technology
Rice University

Stephen J. Pennycook
Douglas H. Lowndes
Oak Ridge National Laboratory

Sivaram Arepalli
G. B. Tech./NASA Johnson Space Center
2101 NASA Road One
Houston, TX 77058

Carter Kittrell
Saujan Sivaram
Myung Kim
Gerry Lavin
Junichiro Kono
Robert Hauge
Richard E. Smalley
Center for Nanoscale Science and Technology
Rice University

**To whom correspondence should be addressed. E-mail: odg@ornl.gov*

References and Notes

1. R. R. Schlittler *et al.*, *Science* **292**, 1136 (2001).
2. A silicon nitride membrane with 350-nm-diameter holes on a 1-μm pitch (Aquamarijn MicroFiltration) was mounted in contact with a Mo TEM grid for use as a shadow mask. Nickel was e-beam-vaporized from an alumina crucible (Thermionics), and C_{60} (MER, sublimed 99.5%) was sublimed from a thermal

evaporation source at normal incidence to the mask and grid to avoid shadow effects. The base pressure during deposition was $< 10^{-7}$ Torr. The deposition rate was monitored using a quartz crystal thickness controller (Maxtek).

3. For high magnetic fields, grids were resistively heated inside 6-mm o.d. quartz tubing (at $<5 \times 10^{-6}$ Torr), which was inserted in the bore of a 7.04 T superconducting magnet (Oxford Instruments). Grids were oriented both parallel and perpendicular to the field axis. Grids were also annealed under zero field conditions using a button heater positioned inside a high vacuum chamber (5×10^{-8} Torr).
4. J. Yuan, L. M. Brown, *Micron* **31**, 515 (2000).
5. O. Stephan *et al*., *J. Electron Spectrosc. Relat. Phenom*. **114–116**, 209 (2001).
6. In an attempt to understand the source of the different contrast between bright and dark layers in the Z-contrast images (Fig. 2E), EELS line traces across several of these layers were averaged to obtain better statistics. However, spectra from the light and dark layers did not reveal a significant compositional change. The most likely explanation is that the crystals we studied were not oriented close enough to a low-index zone axis to reveal the full projected structure, and the contrast variations are the result of channeling variations in the layers.
7. See, for example, (*15*). We have found references of 20 elements incorporated in molybdenum oxide.
8. U. Steiner, W. Reichelt, *Z. Naturforsch*. **52**, 1169 (1997).
9. K.-H. Lii, thesis, Iowa State University (1985).
10. The $Ca_{5.45}Mo_{18}O_{32}$ compound is reported (*9*) to have monoclinic symmetry (space group C2/m) with a = 24.21Å, b = 2.85Å, c = 9.87Å, $\alpha = 90$, $\beta = 109.82$, $\gamma = 90$.
11. For example, the simulations show that when tilting $Ca_{5.45}Mo_{18}O_{32}$ from the [011] projection to the [041] projection, one principal reflection (the {200} reflection with d = 1.14 nm) remains constant while the spacing of the other principal reflection decreases from d = 0.28 nm at the [011] zone axis to d = 0.19 nm at the [041] zone axis. Tilting from the [130] zone axis to the [031] zone axis causes the principal reflection with the larger d-spacing to vary from 0.93 nm to 1.14 nm.
12. The x-ray data used to determine the atomic coordinates for $Ca_{5.45}Mo_{18}O_{32}$ indicate that the formula for complete calcium occupation is $Ca_8Mo_{18}O_{32}$; thus, the Ca positions are 68% occupied (*9*). The most likely explanation for the superlattice reflections is additional structural order associated with partial occupation of the Ca sites. Although partial occupancy was included in the diffraction simulations, ordering of the occupied and unoccupied Ca sites was not.
13. W. K. Hsu *et al*., *Appl. Phys. A* **68**, 493 (1999).
14. D. B. Geohegan *et al*., *Appl. Phys. Lett*. **78**, 3307 (2001).
15. C. C. Torardi, R. E. McCarley, *J. Solid State Chem*. **37**, 393 (1981).
16. We gratefully acknowledge the assistance of J. K. Gimzewski at UCLA for extensive discussions and guidance regarding sample preparation and annealing treatments.

12 November 2002; accepted 2 April 2003